Materials Science in Semiconductor Processing 210 (2026) 110679

Contents lists available at ScienceDirect

Materials Science in Semiconductor Processing

journal homepage: www.elsevier.com/locate/mssp

Dose-response and trap kinetics of Dy^{3+}-doped $LiCa_4O(BO_3)_3$ for thermoluminescence dosimetry

K. Bulcar [a], E.A. Cin [b], Jabir Hakami [c], Abeer S. Altowyan [d,**], M.B. Coban [e,f], U.H. Kaynar [g], M. Topaksu [h], N. Can [c,*]

[a] Igdir University, Vocational School of Health Services, Karaagac Campus, 76000, Igdir, Türkiye
[b] Bakırcay University, Graduate School of Natural and Applied Sciences, Menemen, Izmir, Türkiye
[c] Jazan University, College of Science, Department of Physical Sciences, Physics Division, P.O. Box 114, 45142, Jazan, Kingdom of Saudi Arabia
[d] Department of Physics, College of Science, Princess Nourah Bint Abdulrahman University, P.O. Box 84428, Riyadh, 11671, Saudi Arabia
[e] Balikesir University, Faculty of Arts and Sciences, Department of Physics, Balikesir, Turkiye
[f] Balikesir University, Science and Technology Application and Research Center, Balikesir, Turkiye
[g] Bakircay University, Faculty of Engineering and Architecture, Department of Fundamental Sciences, Menemen, Izmir, Türkiye
[h] Physics Department, Cukurova University, Arts-Sciences Faculty, 01330, Adana, Türkiye

ARTICLE INFO

Keywords:
$LiCa_4O(BO_3)_3:Dy^{3+}$
Thermoluminescence
Mixed trap hierarchy
Two-stage fading
Radiation dosimeter

ABSTRACT

$LiCa_4O(BO_3)_3:Dy^{3+}$ (0.5 wt%) phosphors were investigated as potential thermoluminescent (TL) dosimeters under β irradiation. Following preheating at 155 °C for 10 s and readout at 2 °C s^{-1}, the material exhibits a well-resolved main dosimetric peak at ~185 °C whose maximum temperature remains essentially independent of dose between 1.4 and 150.1 Gy. The integrated TL signal and peak intensity follow a power-law dose dependence ($I \propto D^b$) with exponents $b \approx 1.07$–1.16, indicating an extended quasi-linear response with slight supralinearity at higher doses. Variable heating rate analyses using the Hoogenstraaten and Booth–Bohun–Parfianovitch formalisms yield consistent activation energies of $E \approx 0.86$–1.6 eV and frequency factors on the order of 10^{13} s^{-1}, supporting the presence of a relatively deep and thermally stable dosimetric trap. T_m–T_{stop} and E–T_{stop} analyses reveal a mixed trap hierarchy with stepwise quasi-stable energy intervals, indicative of thermally grouped shallow, intermediate and deep trapping regions. Computerized glow-curve deconvolution resolves the composite glow curve into ten general-order components (≈0.85–1.65 eV) prior to preheating, which reduce to five deeper components (≈1.44–1.67 eV) after thermal cleaning, consistent with the suppression of shallow traps and the dominance of stable dosimetric levels. Post-irradiation storage exhibits a two-stage temporal evolution of the ~185 °C peak, characterized by early intensity build-up followed by long-term fading while T_m remains constant, behaviour consistent with charge redistribution within a mixed-trap framework. Overall, the results indicate that $LiCa_4O(BO_3)_3:Dy^{3+}$ combines a thermally robust main peak, extended quasi-linear dose response, and low effective atomic number, supporting its potential for tissue-equivalent TL dosimetry.

1. Introduction

Borate-based phosphors have attracted sustained interest in luminescence dosimetry owing to their good thermal and chemical stability, relatively low effective atomic number, ease of preparation, and favorable storage characteristics after irradiation, which together support accurate dose recording over a wide range of conditions [1–3]. Numerous borate hosts, including lithium borates and complex rare-earth borates, have been explored for TL applications, where detailed glow curve analysis and kinetic characterization enable optimization of dosimetric performance [4,5].

Within this class, rare-earth-doped borates have proven particularly promising because the host lattice can accommodate a rich defect structure while activator ions introduce efficient recombination centres and tune trap distributions relevant for TL [6,7]. Dysprosium is a widely used activator in oxide and borate phosphors; Dy^{3+} incorporation often generates suitable electron and hole traps, yields intense TL signals with useful dose–response behaviour, and supports acceptable fading and

* Corresponding author.
** Corresponding author
E-mail addresses: asaltowyan@pnu.edu.sa (A.S. Altowyan), ncan@jazanu.edu.sa (N. Can).

https://doi.org/10.1016/j.mssp.2026.110679
Received 27 February 2026; Received in revised form 21 March 2026; Accepted 9 April 2026
Available online 16 April 2026

reusability characteristics for dosimetric applications [8–11]. Dy^{3+}-doped borate and borate-related hosts have shown linear or extended quasi-linear dose response, low detection thresholds, and stable TL peaks amenable to kinetic analysis via methods such as variable heating rate, initial rise and glow curve deconvolution [12,13].

The Li–Ca–borate family is an attractive platform in this context. $LiCaBO_3$ has already been identified as a versatile TL and photoluminescent host, with rare-earth doping enabling efficient emission, tunable glow curves and satisfactory dosimetric characteristics [5,14]. More complex Li–Ca borates, such as $Li_4Ca(BO_3)_2:Dy^{3+}$, exhibit well-defined TL peaks under UV exposure, dose-dependent peak shifts indicative of non-first-order kinetics, and measurable optical and thermal fading behavior, highlighting the potential of Li–Ca borates for radiation detection [9]. These results suggest that lithium–calcium borate frameworks provide a flexible structural environment for stabilizing Dy^{3+}-related traps and tailoring TL performance via compositional design.

$LiCa_4O(BO_3)_3$ belongs to the broader $A_4REO(BO_3)_3$-type borate family, which has recently emerged as a robust host system for luminescent and dosimetric materials. Tb^{3+}- and Sm^{3+}-doped $LaCa_4O(BO_3)_3$ and related $Ca_4LaO(BO_3)_3$ or $YCa_4O(BO_3)_3$ compounds display complex glow curve structures with high temperature dosimetric peaks, anomalous or non-trivial heating rate behavior, good reusability, and linear or extended dose response, supporting their suitability for TL dosimetry and providing a rich platform for kinetic modelling [15,16]. These findings indicate that the $Ca_4REO(BO_3)_3$-type borate framework can host multiple, thermally well-separated traps and recombination centres, making $LiCa_4O(BO_3)_3$ a particularly promising candidate where the presence of Li^+ may additionally favor efficient charge transport and trap formation.

In rare-earth–doped borates, Dy^{3+} typically substitutes on trivalent cation sites and participates in charge-compensated defect complexes involving oxygen vacancies or monovalent cations, which act as electron/hole traps controlling TL peak position and kinetics [17]. In Li-containing hosts, the high mobility and charge flexibility of Li^+ can modify the trap depth spectrum and promote coupling between shallow and deep traps. In $Ca_4REO(BO_3)_3$–type lattices, the presence of multiple cation sublattices is expected to generate a complex trap hierarchy, potentially responsible for high-temperature dosimetric peaks and non-first-order behavior [18].

Understanding how Dy^{3+}-related defect complexes shape the trap depth distribution and recombination pathways is essential for controlling fading behavior. In Dy-doped borate hosts, Dy-centred complexes and oxygen-related defects generate a spectrum of shallow and deep traps that govern both initial TL sensitivity and time-dependent signal loss, with concentration-dependent changes in peak position and kinetic order reported for $Li_4Ca(BO_3)_2:Dy^{3+}$ and other Dy-activated borates [19,20].

From a dosimetric standpoint, suitable trap depths, low fading, linear dose response and near-tissue effective atomic number ($Z_{eff} \approx 7$–10) are key performance criteria [2,21]. Recent Dy-doped low-Z borate systems such as Al–Li–Zn borate, $LiMgBO_3:Dy^{3+}$ and MgB_4O_7:RE have demonstrated good linearity, low room temperature fading and Z_{eff} close to soft tissue or bone [20,22].

Although Dy^{3+} has been extensively studied as a TL activator in various borate and oxide hosts, and detailed kinetic analyses have been carried out for several members of the RE–$Ca_4O(BO_3)_3$ family, there is a clear lack of systematic TL and kinetic investigations for Dy^{3+}-doped $LiCa_4O(BO_3)_3$. In particular, no comprehensive study has yet addressed the dose-response characteristics, heating-rate dependence, reusability and fading behavior, together with a consistent multi-method kinetic analysis (VHR, IR, T_m–T_{stop} and CGCD) across different Dy^{3+} concentrations in this host.

The present work aims to fill this gap by (i) synthesizing $LiCa_4O(BO_3)_3:xDy^{3+}$ phosphors with varying Dy^{3+} concentrations and confirming the phase purity of the host lattice, (ii) characterizing the TL glow curve structure under ionizing radiation and evaluating the dose–response behavior over a broad dose range, (iii) examining the influence of heating rate, reusability and storage (fading) on the main dosimetric peak(s), and (iv) performing a detailed TL kinetic analysis using the Variable Heating Rate, Initial Rise, T_m–T_{stop} and CGCD approaches to determine trap parameters and elucidate the trap–recombination scheme as a function of Dy^{3+} content. It is hypothesized that Dy^{3+} incorporation in $LiCa_4O(BO_3)_3$ modifies the trap depth distribution and recombination kinetics via charge-compensated defect complexes involving cation sublattices and oxygen vacancies, leading to systematic, concentration-dependent changes in TL peak position, kinetic order and fading behavior.

2. Sample preparation and characterization techniques

Dy^{3+}-activated $LiCa_4O(BO_3)_3$ phosphors were synthesized via a sol–gel assisted combustion method using urea as a fuel agent. The starting materials were lithium nitrate ($LiNO_3$, Sigma-Aldrich, ≥99.99%), calcium nitrate hydrate ($Ca(NO_3)_2{\cdot}xH_2O$, Sigma-Aldrich, ≥99.9%), boric acid (H_3BO_3, Merck, ≥99.5%), and urea ($CO(NH_2)_2$, Merck, ≥99.0%). Dysprosium nitrate hydrate ($Dy(NO_3)_3{\cdot}xH_2O$, Sigma-Aldrich, 99.9% trace metals basis) was used as the activator precursor. All chemicals were used as received without further purification. The Dy^{3+} concentration was varied at 0.5, 1, 2, 3, 5, and 7 wt% relative to the host composition. In a typical preparation, stoichiometric amounts of $LiNO_3$ and $Ca(NO_3)_2$ were dissolved in 20 mL of deionized water under continuous magnetic stirring. Boric acid was then added, followed by the required amount of $Dy(NO_3)_3$ to achieve the desired dopant concentration. Urea was introduced to maintain the appropriate fuel-to-oxidizer balance required for a self-sustaining combustion reaction. The solution was heated at ~80 °C under constant stirring for approximately 1 h to ensure complete dissolution and compositional homogeneity. Upon gradual evaporation of excess solvent, a viscous gel was obtained. This gel was subjected to microwave irradiation, triggering rapid combustion accompanied by gas release and formation of a porous precursor powder. The as-combusted powders were subsequently calcined in air at 800 °C for 2 h to improve crystallinity and remove residual organic species. The heating rate during calcination was fixed at 5 °C min^{-1}, and the furnace was allowed to cool naturally to room temperature. The resulting fine powders were stored in a desiccator until structural and TL characterization.

Phase identification and crystallographic analysis were carried out using X-ray diffraction (XRD) with Cu Kα radiation (λ = 1.5406 Å), operated at 40 kV and 40 mA. Diffraction patterns were collected in the 2θ range of 10°–80° with a step size of 0.02°. TL measurements were performed using a Lexsyg Smart TL/OSL reader (Freiberg Instruments, Germany) equipped with an internal $^{90}Sr/^{90}Y$ beta irradiation source providing a nominal dose rate of ~1.436 Gy s^{-1}. Approximately 23.8 mg of powder was pressed into 6 mm diameter pellets to ensure reproducible geometry and stable thermal contact during heating. After irradiation, samples were heated from room temperature to 450 °C under a linear heating regime. A reference heating rate of 2 °C s^{-1} was applied for standard glow curve acquisition. All TL measurements were conducted under continuous nitrogen flow to minimize oxidation and suppress parasitic chemiluminescence.

3. Results and discussions

3.1. Structural properties

Fig. 1 presents the XRD patterns of undoped and Dy^{3+}-doped LiCBO phosphors (0.02 and 0.05 mol). All diffraction peaks can be indexed to the standard LiCBO pattern (JCPDS card no. 98-009-9386), confirming the formation of a single-phase LiCBO structure without any detectable secondary phases.

The main reflections located at $2\theta \approx 15°$, 27°, 29°, 31°, 34°, 38°,

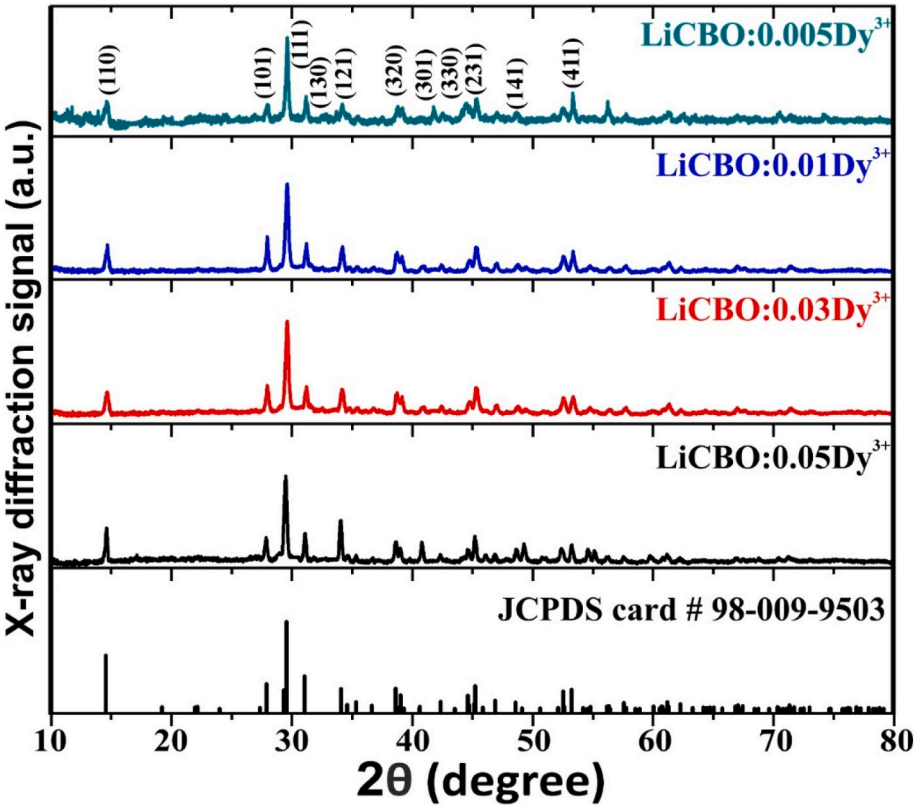

Fig. 1. X-ray diffraction (XRD) patterns of Dy^{3+}-doped LiCBO phosphors with different Dy^{3+} concentrations (0.005, 0.01, 0.03, and 0.0). All diffraction peaks are consistent with the standard data (JCPDS card no. 98-009-9503).

45°and 53° are characteristic of the LiCBO lattice planes. The overall diffraction profiles remain essentially unchanged upon Dy^{3+} incorporation, indicating that the host crystal structure is retained after doping. Given the similar ionic radii and compatible coordination environments, Dy^{3+} ions are expected to substitute Ca^{2+} sites in the LiCBO lattice. The heterovalent substitution of Ca^{2+} by Dy^{3+} induces slight lattice distortions due to both ionic size and charge mismatch, which is evidenced by the small systematic shifts in the peak positions with increasing Dy^{3+} content. Charge compensation is most likely achieved through the formation of intrinsic lattice defects, such as cation vacancies (e.g. Li^{+} vacancies) or associated defect complexes. The presence of sharp and well-defined diffraction peaks for all compositions indicates good crystallinity of the synthesized samples.

3.2. *Spectral detection, Dy^{3+} concentration and preheating effects on TL glow curves*

Fig. 2a shows the TL glow curves of $LiCa_4O(BO_3)_3:Dy^{3+}$ (0.5 wt%) recorded after 20 Gy irradiation using the BSL–TL 365 nm, IRSL–TL 410 nm, and IRSL–TL 565 nm filter combinations [23]. Although the overall glow curve structure remains similar for all detection windows, the highest intensity is observed with the IRSL–TL 565 nm filter, indicating that the dominant TL signal is detected in the Dy^{3+} emission region.

The glow curve recorded under the IRSL–TL 565 nm filter (Fig. 2b) exhibits a distinct peak at approximately 75 °C, a pronounced shoulder around 112 °C, and a broader glow region centred near 182 °C. The presence of multiple thermally resolved components is consistent with a distribution of trap depths. Such composite glow structures are commonly associated with overlapping trapping states and possible trap–recombination centre interactions, although detailed kinetic analysis would be required for definitive identification [24,25]. The asymmetry and peak overlap suggest deviation from ideal first-order kinetics, potentially reflecting re-trapping processes and competitive recombination between closely spaced trap levels.

Fig. 2c presents the TL response as a function of Dy^{3+} concentration (0–7 wt%), measured with the IRSL–TL 565 nm filter. At concentrations below 0.5 wt%, the TL intensity is markedly reduced, indicating insufficient activator density for efficient TL signal generation. The intensity increases with Dy^{3+} content and reaches a maximum at approximately 0.5–1 wt%, defining the optimum concentration range for sensitivity. At higher concentrations, the intensity decreases systematically. This behaviour is consistent with concentration quenching and/or Dy–Dy interactions, which may modify the defect environment and reduce TL efficiency [26–28], possibly through the formation of Dy-related defect clusters that alter local charge-compensation conditions.

Such concentration-dependent behaviour is consistent with a defect-controlled TL mechanism, in which Dy^{3+} ions influence both recombination probability and trap structure [10,29]. In this framework, Dy^{3+} incorporation may affect not only the density of recombination centres but also the spatial correlation between traps and luminescent centres, leading to mixed-trap structures. However, alternative or concurrent mechanisms, such as cross-relaxation processes or changes in intrinsic trap populations with increasing Dy^{3+} content, may also contribute [30,31], particularly at higher dopant concentrations where non-radiative energy transfer pathways become more probable.

In order to further probe the stability of the trapping system, preheating experiments were performed prior to TL readout. As shown in Fig. 2d, the TL glow curves recorded after progressive preheating exhibit a systematic reduction of low temperature components, while higher temperature features persist up to their respective thermal stability limits. Fig. 2d (inset) shows the corresponding variation of the integrated glow curve area as a function of preheat temperature, clearly indicating the progressive removal of shallow and thermally unstable trap contributions [13,15]. This behaviour is characteristic of borate-based TL phosphors exhibiting multi-trap structures with thermally separated glow components. As the preheat temperature

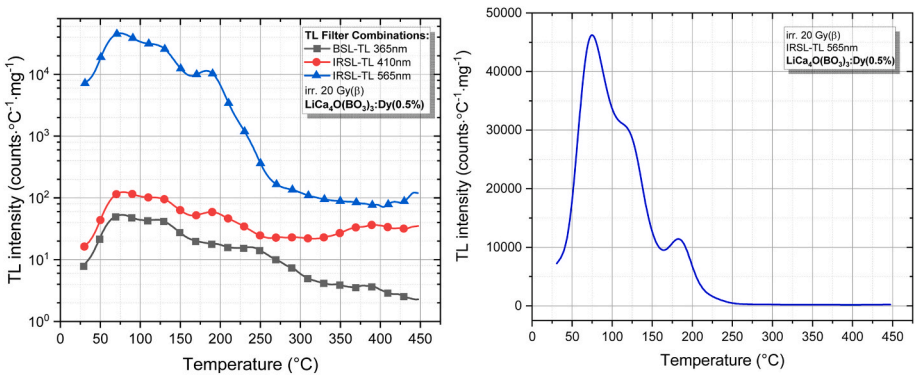

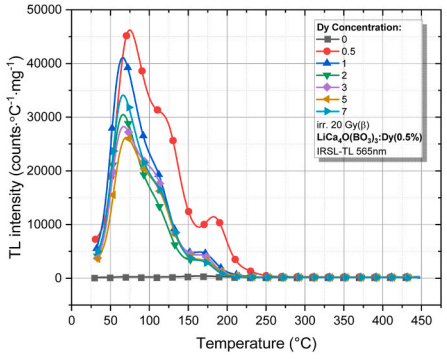

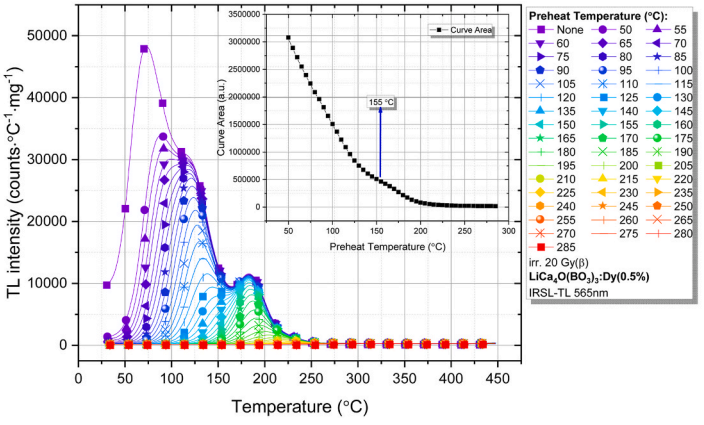

Fig. 2. (a) TL glow curves of $LiCa_4O(BO_3)_3:Dy^{3+}$ (0.5 wt%) recorded after 20 Gy irradiation using different optical filter combinations (BSL–TL 365 nm, IRSL–TL 410 nm, and IRSL–TL 565 nm). (b) TL glow curve of $LiCa_4O(BO_3)_3:Dy^{3+}$ (0.5 wt%) recorded with the IRSL–TL 565 nm filter, showing a main peak at ~75 °C, a shoulder around ~112 °C, and a broader glow region near ~182 °C. (c) TL glow curves recorded with the IRSL–TL 565 nm filter as a function of Dy^{3+} concentration (0–7 wt%) under 20 Gy irradiation (d) TL glow curves recorded after progressive preheating at different temperatures prior to readout (IRSL–TL 565 nm), illustrating the systematic removal of low-temperature components; inset: variation of the integrated TL glow curve area as a function of preheat temperature.

increases, carriers stored in the shallower portion of this distribution are thermally released before the main readout, leading to a progressive reduction in the integrated TL signal. The asymmetric and partially overlapping glow curve structure suggests deviation from ideal first-order kinetics, implying retrapping and competitive recombination processes. In complex borate lattices, such behaviour has been associated with defect clustering and mixed-trap interactions [32]. Under these conditions, preheating may not only empty shallow traps but also slightly redistribute charge among remaining deeper traps prior to readout. The pronounced reduction in integrated area above ~150–160 °C is consistent with the onset of depletion of traps contributing to the broader ~182 °C region, marking a transition from selective shallow-trap cleaning to progressive depletion of traps relevant for dosimetric stability. On this basis, a preheating temperature of 155 °C for 10 s was selected as an optimized condition within this transition region, ensuring effective suppression of shallow and thermally unstable trap contributions while preserving the integrity of the deeper, thermally stable dosimetric traps. Overall, the preheat-dependent area loss is

dominated by thermal emptying of progressively deeper traps, while its detailed temperature dependence is influenced by mixed-trap kinetics inherent to the $LiCa_4O(BO_3)_3:Dy^{3+}$ system.

3.3. Dose–response behaviour and kinetic implications of the main dosimetric peak

As shown in Fig. 3a, the β-irradiated TL glow curves of $LiCa_4O(BO_3)_3:Dy^{3+}$ (0.5 wt%) measured with IRSL–TL 565 nm after preheating at 155 °C for 10 s are dominated by a well-resolved main dosimetric peak centred at ~185 °Cover the investigated dose range of 1.4–150.1 Gy. The peak maximum temperature (T_m) remains essentially unchanged with increasing dose, while the peak intensity increases systematically. The corresponding irradiation times ranged from approximately 1 s to 105 s for the applied dose interval, based on the dose rate of the internal $^{90}Sr/^{90}Y$ β source (~1.436 Gy s^{-1}). Under these conditions, the influence of fading during irradiation is expected to be negligible. This can be attributed to the fact that the analysed TL signal is dominated by the thermally stable high-temperature dosimetric peak (~185 °C), associated with relatively deep trapping levels that are not significantly affected by short-term thermal release at room temperature. Furthermore, no observable shift in the peak maximum temperature (T_m) with increasing dose was detected, indicating that the trap structure remains stable and is not influenced by irradiation-time-dependent effects.

This invariance of T_m indicates that the trap depth associated with the ~185 °C peak is not significantly affected by increasing trap occupancy under the present irradiation conditions.

The dose–response characterization was performed in the range 1.4–150 Gy in order to ensure reliable and reproducible measurements of the thermally stable high-temperature TL peak (~185 °C). This dose interval provides a sufficiently high signal-to-noise ratio for accurate kinetic and dose–response analysis. At lower doses (<1 Gy), the TL signal associated with the deep dosimetric traps becomes comparatively weak under the present experimental conditions, which reduces the reliability of quantitative evaluation. Furthermore, the analysis focuses on the thermally stable high-temperature peak, while low-temperature components were excluded due to their rapid fading and limited dosimetric relevance. At very low doses, the relative contribution of such

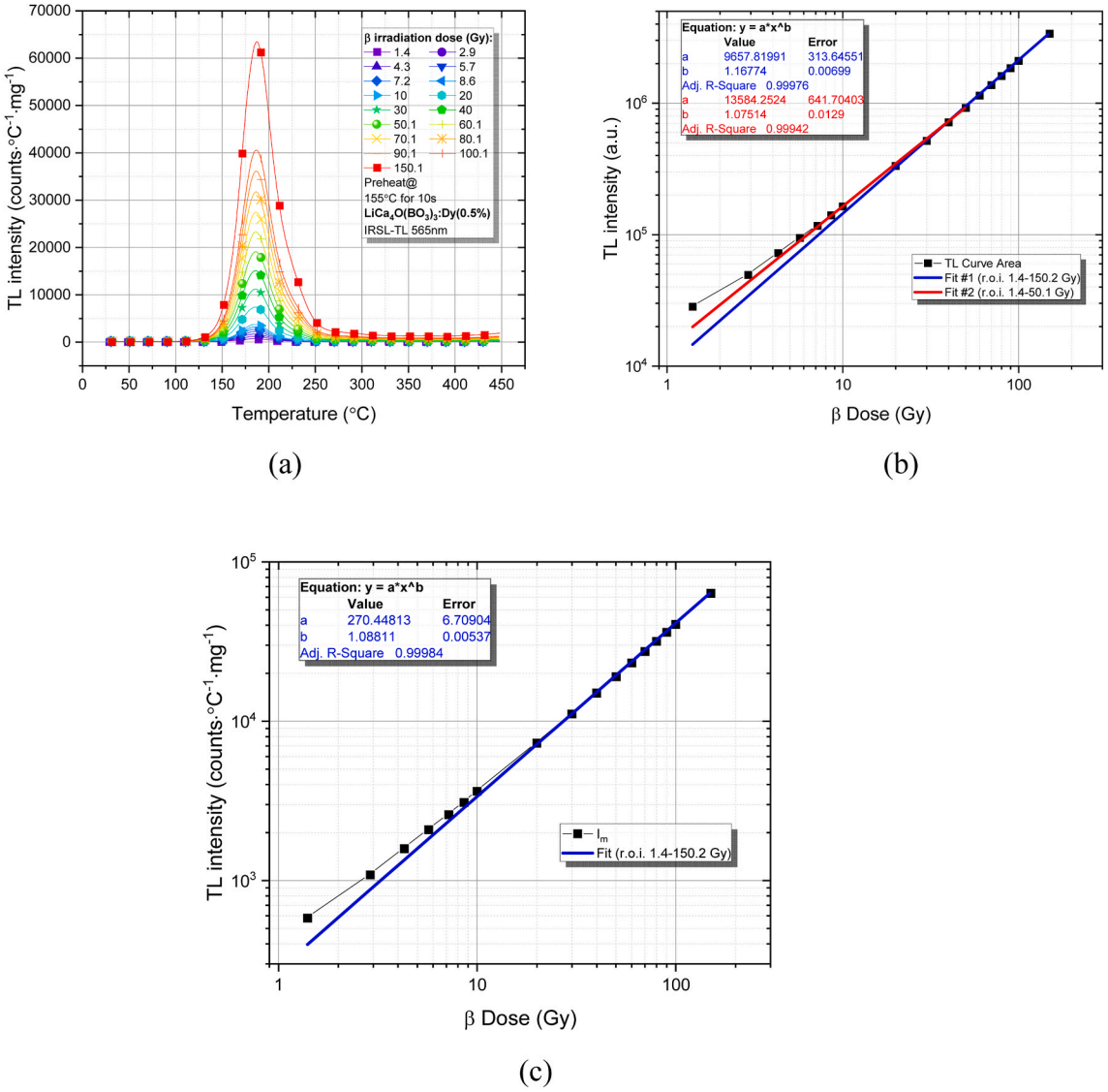

Fig. 3. (a) TL glow curves of $LiCa_4O(BO_3)_3:Dy^{3+}$ (0.5 wt%) recorded under IRSL–TL 565 nm detection following β-irradiation over the dose range 1.4–150.1 Gy (preheated at 155 °C for 10 s prior to readout), showing systematic intensity increase with dose. (b) Dose–response behaviour of the integrated TL glow-curve area as a function of β dose (1.4–150.2 Gy) plotted on a log–log scale, fitted using a power-law function ($y = a \cdot x^b$), indicating near-linear response. (c) Dose–response behaviour of the main peak intensity (I_m) as a function of β dose in the same range, also fitted with a power-law function, demonstrating quasi-linear dependence with high correlation.

unstable components becomes more pronounced, which is not consistent with the scope of the present study.

The dose dependence of the integrated TL signal is presented in Fig. 3b, where the log–log plot of integrated glow curve area versus dose is well described by a power-law function $y = a \cdot x^b$ with $b \approx 1.07$ and $R^2 \approx 0.999$. Similarly, the dose dependence of the main peak intensity (I_m) shown in Fig. 3c yields $b \approx 1.09$ with comparable correlation. These near-unity exponents demonstrate an extended quasi-linear response over more than two decades of dose, with only slight supralinearity at higher doses. No evident saturation or peak distortion is observed within the studied interval up to ~150.1 Gy.

The combination of a dose-stable peak position (Fig. 3a) and quasi-linear intensity increase (Fig. 3b and c) suggests the presence of a thermally stable dosimetric trap governing the ~185 °C emission. From a kinetic standpoint, the absence of significant peak shift with increasing dose is commonly associated with first-order or low-retrapping general-order kinetics, where the peak temperature remains largely independent of the initial trap population. The slight supralinearity ($b > 1$) indicates limited retrapping or weak competition effects during trap filling, suggesting behaviour closer to quasi-first-order kinetics rather than strictly ideal first-order behaviour.

However, definitive identification of the kinetic order of the ~185 °C peak requires dedicated kinetic analysis. VHR and IR methods can test for order-dependent shifts in T_m and enable extraction of activation energies, while comparison of experimental peak shape factors with theoretical predictions allows discrimination between first- and general-order kinetics. In addition, CGCD would be necessary to resolve potential overlapping components and quantitatively evaluate retrapping effects within the mixed-trap framework inferred for $LiCa_4O(BO_3)_3:Dy^{3+}$.

Overall, Fig. 3a–c collectively demonstrate that $LiCa_4O(BO_3)_3:Dy^{3+}$ exhibits a stable main dosimetric peak at ~185 °C with extended quasi-linear dose response and kinetic features consistent with low-retrapping general-order or quasi-first-order behaviour, supporting its suitability for dosimetric applications.

3.4. Heating-rate dependence and kinetic interpretation of the main TL peak

Fig. 4a–c presents the influence of heating rate (0.5–5 °C s^{-1}) on the main TL peak of $LiCa_4O(BO_3)_3:Dy^{3+}$ (0.5 wt%) centred at ~185 °C under IRSL–TL 565 nm detection following 20 Gy β-irradiation. As shown in Fig. 4a, the peak maximum temperature (T_m) shifts

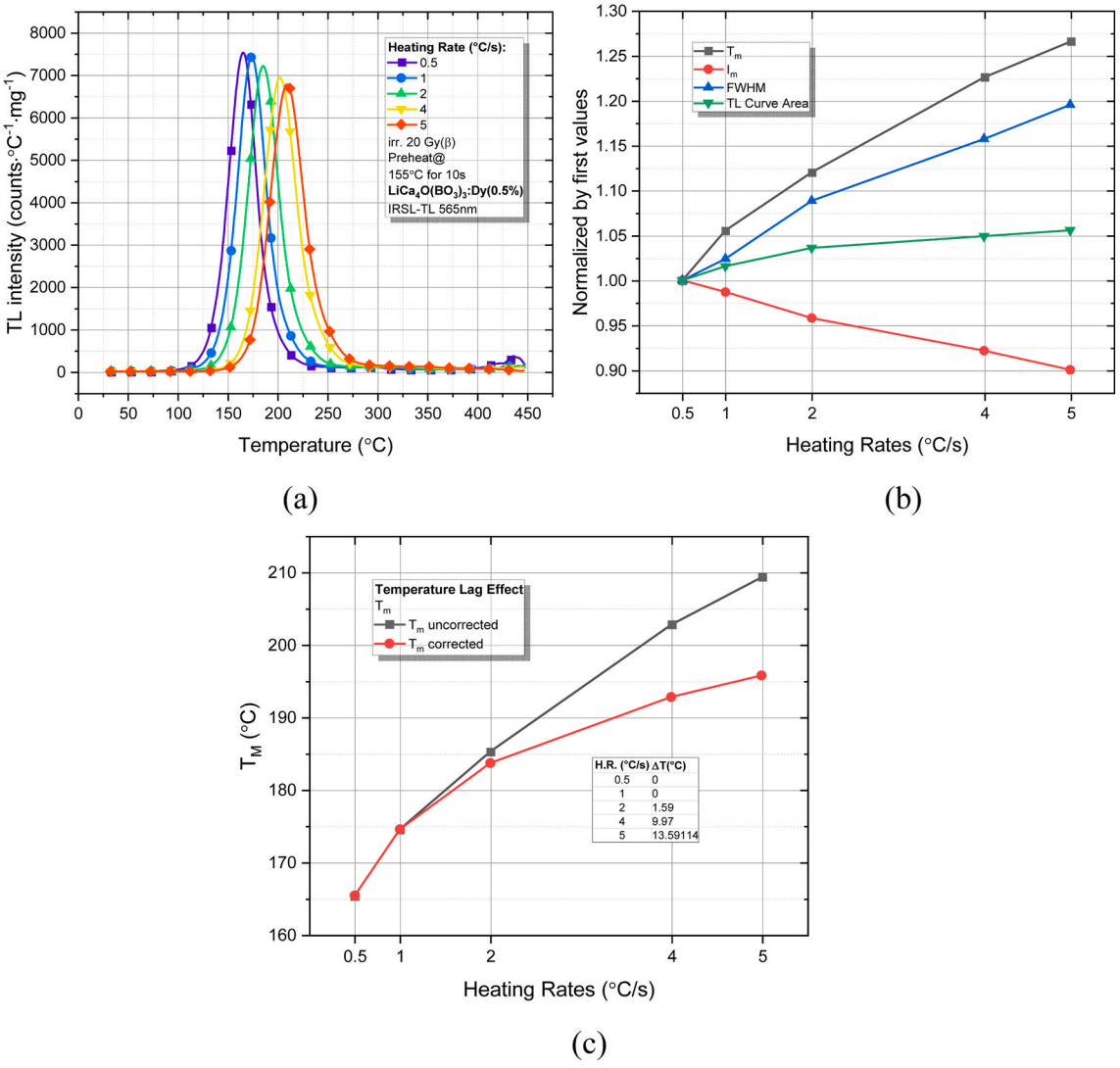

Fig. 4. (a) TL glow curves of $LiCa_4O(BO_3)_3:Dy^{3+}$ (0.5 wt%) recorded under IRSL–TL 565 nm detection at different heating rates (0.5–5 °C s^{-1}) after 20 Gy β-irradiation, showing systematic shift of the main peak towards higher temperatures with increasing heating rate. (b) Variation of normalized peak parameters (T_m, full width at half maximum (FWHM), and integrated glow-curve area) as a function of heating rate, illustrating heating-rate-dependent peak broadening and intensity changes. (c) Dependence of peak maximum temperature (T_m) on heating rate; both uncorrected and thermally corrected T_m values.

systematically toward higher temperatures with increasing heating rate. Simultaneously, the full width at half maximum (FWHM), integrated area, and normalized peak parameters exhibit smooth heating-rate-dependent trends (Fig. 4b) [33].

The systematic displacement of T_m with increasing heating rate is a characteristic feature of thermally activated release processes within the Randall–Wilkins formalism. Both first-order and general-order kinetics predict such heating-rate dependence, with T_m typically exhibiting an approximately logarithmic dependence on β [34]. The near-logarithmic trend observed for both uncorrected and thermally corrected T_m values in Fig. 4c is therefore consistent with a dominant trap governing the ~185 °C peak and supports the applicability of the VHR method for activation energy determination [35,36]. Temperature-lag corrections were applied to the measured T_m values following the method proposed by Kitis and Tuyn [37], which accounts for the dependence of apparent peak temperature on heating rate. To account for the apparent shift of the glow peak temperature with increasing heating rate, the temperature lag effect was evaluated using a standard logarithmic correction approach following Kitis and Tuyn [37]. The corrected peak temperature T_{mj} corresponding to a heating rate β_j was calculated relative to a reference heating rate β_i according to the relation:

$$T_{m_j} = T_{m_i} - \frac{T_{m_2} - T_{m_1}}{ln\left(\frac{\beta_2}{\beta_1}\right)} ln\left(\frac{\beta_i}{\beta_j}\right) \quad (1)$$

where T_{mi} and T_{mj} represent the peak temperatures at heating rates β_i and β_j, respectively, and T_{m1} and T_{m2} correspond to two selected reference heating rates β_1 and β_2. This correction accounts for the delay between the nominal heater temperature and the actual sample temperature, which becomes more pronounced at higher heating rates.

The temperature-lag parameter was effectively determined by analysing the systematic variation of T_m with heating rate and minimizing the dispersion in the extracted activation energy values. The corrected temperatures were then used in subsequent kinetic analyses to obtain more consistent and physically meaningful estimates of the activation energy.

The modest increase in FWHM with increasing β suggests slight peak broadening relative to an ideal single-trap first-order system, where peak shape would remain strictly invariant. Such behaviour is commonly associated with low-retrapping general-order kinetics or with partially overlapping components in mixed-trap systems. In rare-earth-doped borate hosts, complex glow curve structures and coupled shallow–deep trap hierarchies have frequently been reported, leading to effective kinetic orders marginally above unity under varying heating conditions.

The systematic yet smooth variation of integrated area and normalized peak parameters with β further indicates that the ~185 °C peak remains thermally stable and structurally coherent over the studied heating-rate range. The absence of anomalous peak distortion or irregular intensity enhancement suggests operation within the conventional quasi-equilibrium regime, where VHR analysis yields reliable estimates of trap parameters provided that temperature lag and thermal quenching effects are properly accounted for.

3.5. Reusability

The 15-cycle TL measurements shown in Fig. 5a and b demonstrate a highly reproducible dosimetric response of $LiCa_4O(BO_3)_3:Dy^{3+}$ (0.5 wt %) under identical irradiation and readout conditions. As observed in Fig. 5a, the main dosimetric peak at ~185 °C is retained with essentially unchanged peak position throughout all consecutive cycles, indicating that the associated trapping level remains thermally stable under repeated use and that no observable structural modification occurs within the applied readout protocol.

The cycle-to-cycle variation of the normalized main-peak intensity presented in Fig. 5b remains within ±5, which lies within typical experimental variability [38]. This behaviour demonstrates good readout reproducibility with negligible sensitivity degradation over repeated irradiate–preheat–read sequences.

Together with the previously established dose-stable peak position and quasi-linear dose response of the ~185 °C peak, these results suggest that the dominant trapping level exhibits sufficient thermal robustness and resistance to cumulative thermal and irradiation effects. Overall, $LiCa_4O(BO_3)_3:Dy^{3+}$ (0.5 wt%) demonstrates good reusability, acceptable cycle-to-cycle reproducibility, and suitability for routine TL dosimetric applications.

4. Kinetic analysis

4.1. Heating-rate-based kinetic analysis of the main TL peak

The Hoogenstraaten method determines the activation energy (E) from the heating-rate dependence of the peak maximum temperature (T_m), assuming a logarithmic relationship between T_m and the heating

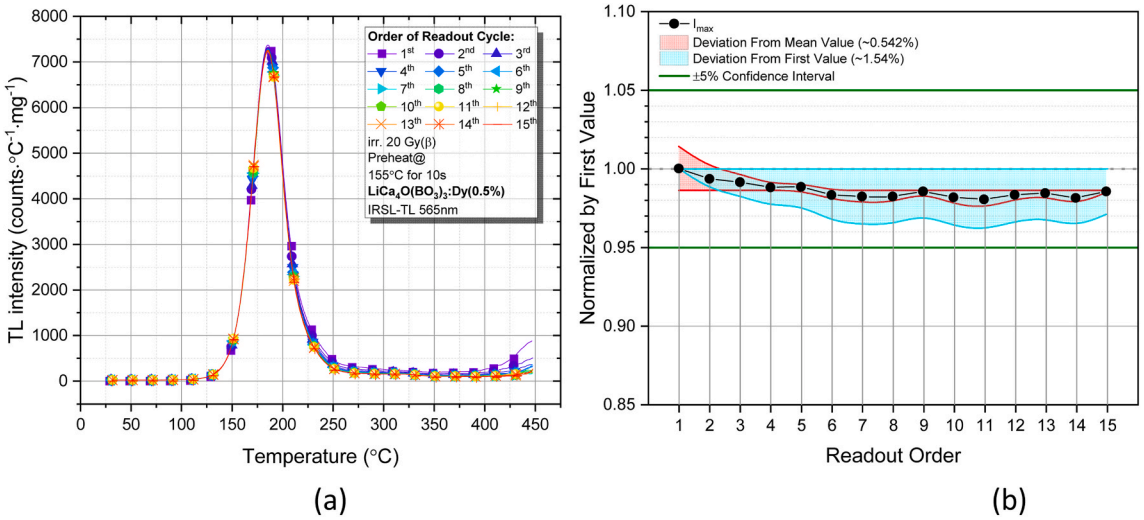

Fig. 5. (a) TL glow curves of $LiCa_4O(BO_3)_3:Dy^{3+}$ (0.5 wt%) recorded under IRSL–TL 565 nm detection over 15 consecutive readout cycles following 20 Gy β-irradiation (preheated at 155 °C for 10 s prior to each measurement), illustrating the reproducibility of the main dosimetric peak at ~185 °C. (b) Cycle-to-cycle variation of the normalized main peak intensity (I_m) as a function of readout number, showing measurement reproducibility within ±5% deviation bands.

rate (β). In this approach, the relation is expressed as

$$ln\left(\frac{T_m^2}{\beta}\right) = \frac{E}{kT_m} + ln\left(\frac{ks}{E}\right) \quad (2)$$

where k is the Boltzmann constant and s is the frequency factor. By plotting $ln(T_m^2/\beta)$ versus $1/T_m$, the activation energy E is obtained from the slope of the resulting linear relation.

The Booth–Bohun–Parfianovitch (BBP) method is an alternative heating-rate approach that evaluates E using pairs of peak temperatures measured at different heating rates. For two heating rates β_1 and β_2, with corresponding peak temperatures T_{m1} and T_{m2}, the activation energy is calculated as

$$E = k\frac{T_{m_1}T_{m_2}}{T_{m_1} - T_{m_2}} ln\left[\frac{\beta_1}{\beta_2}\left(\frac{T_{m_2}}{T_{m_1}}\right)^2\right] \quad (3)$$

This method provides an independent estimate of the activation energy and is commonly used to validate kinetic parameters derived from conventional heating-rate analysis.

The Hoogenstraaten plots constructed from the heating-rate measurements (Fig. 6) exhibit good linearity for both uncorrected and temperature-lag-corrected peak maximum temperatures, indicating that the heating-rate formalism is applicable within the investigated β range (0.5–5 °C s^{-1}) for the ~185 °C dosimetric peak. The linear regression coefficients indicate a well-defined dominant trap group governing this glow peak under the applied experimental conditions.

The activation energy (E) values obtained from the slope of the Hoogenstraaten plots and from the Booth–Bohun–Parfianovitch (BBP) method are summarized in Table 1. Both methods yield comparable E values within experimental uncertainty, supporting the reliability of the extracted kinetic parameters under the assumption of a single dominant peak with limited overlap. As expected, temperature-lag correction results in slightly higher E values, reflecting the systematic shift of measured T_m toward lower apparent temperatures at higher heating rates.

The obtained activation energy (~1.2–1.26 eV, depending on correction) corresponds to a relatively deep trapping level in the context of TL dosimetry and is consistent with thermal stability under room-temperature storage and the applied preheat–readout protocol. The corresponding frequency factor (s) values fall within the typical range reported for rare-earth-doped borate TL phosphors, further supporting the physical plausibility of the derived parameters.

Overall, the agreement between Hoogenstraaten and BBP methods, together with the linear heating-rate behaviour, suggests that the main dosimetric peak of $LiCa_4O(BO_3)_3:Dy^{3+}$ is governed by a well-defined trapping centre exhibiting behaviour consistent with low-retrapping general-order (quasi-first-order) kinetics, rather than conclusively demonstrating strictly ideal first-order behaviour. Definitive determination of kinetic order, however, requires complementary analyses (e.g., peak-shape evaluation, IR method, CGCD) to fully resolve possible overlapping contributions within the mixed-trap framework.

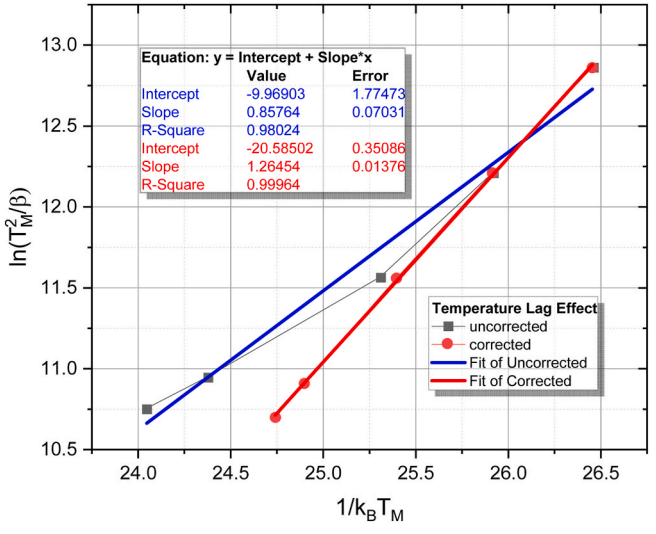

Fig. 6. Hoogenstraaten plot of the main TL peak (~185 °C) of $LiCa_4O(BO_3)_3:Dy^{3+}$ (0.5 wt%) obtained from heating-rate measurements (0.5–5 °C s^{-1}). Linear fits of $ln(T_m^2/\beta)$ versus $1/T_m$ are shown for uncorrected and temperature-lag-corrected data, from which the activation energy (E) and frequency factor (s) were determined.

Table 1
Activation energy (E) of the main TL peak (~185 °C) of $LiCa_4O(BO_3)_3:Dy^{3+}$ (0.5 wt%) determined by Hoogenstraaten and BBP methods using uncorrected and temperature-lag-corrected T_m values. Frequency factors (s) from Hoogenstraaten analysis are also listed.

β (°C/s)	Maximum 1		
	UnCorrected	Corrected	
1	1.20	1.20	
2	1.13	1.23	
4	0.92	1.25	Booth-Bohun-Parfianovitch
5	0.87	1.26	Method
Average E	**1.03 ± 0.16**	**1.24 ± 0.03**	
***E* (eV)**	**0.86 ± 0.07**	**1.26 ± 0.01**	Hoogenstraaten's Method
(0.5–5 °C/s)			
***s* (s^{-1})**	**2.13x10^{8}**	**1.28x10^{13}**	

4.2. T_m–T_{stop} analysis and trap structure interpretation

To further examine the trapping structure of $LiCa_4O(BO_3)_3:Dy^{3+}$ (0.5 wt%), the T_m–T_{stop} method was applied by progressively increasing the T_{stop} temperature prior to each TL readout. The evolution of the glow curves with increasing preheat temperature (Fig. 7a) demonstrates gradual removal of lower-temperature components while higher-temperature structures persist up to their respective stability limits, indicating the presence of multiple trapping levels.

The corresponding T_m–T_{stop} plot (Fig. 7b) exhibits quasi-linear T_m increase in the lower T_{stop} region. Similar behaviour was reported by Benavente et al. for $Li_2B_4O_7$:Cu,Ag, where linear T_m–T_{stop} segments were interpreted as being consistent with a quasi-continuous trap distribution or strongly overlapping discrete trapping levels [39]. Importantly, that study emphasized that T_m–T_{stop} analysis alone cannot uniquely distinguish between continuous trap distributions and closely spaced discrete levels without complementary CGCD and kinetic modelling [40].

In intermediate temperature regions, plateau-like segments of T_m–T_{stop} behaviour are observed, suggesting the temporary dominance of relatively discrete and thermally stable trapping levels. These plateau regions coincide with quasi-stable intervals observed in the E–T_{stop} evolution (Fig. 7c), reinforcing the presence of thermally distinct trap groupings. It should be noted that This behaviour arises solely from the intrinsic stepwise T_{stop} sequence of the T_m–T_{stop} protocol, without any additional independent stabilization preheat. Comparable behaviour has been described in rare-earth-doped borates where T_m–T_{stop}, VHR and CGCD were used jointly to separate overlapping components. However, T_m–T_{stop} behaviour by itself does not provide direct information about kinetic order and should not be interpreted as definitive evidence for first- or general-order kinetics [7,40,41].

Fig. 7c presents the activation energy evolution derived from the T_m–T_{stop} analysis. The E–T_{stop} dependence shows stepwise variations, with lower activation energies obtained at small T_{stop} values and progressively higher energies emerging as deeper trap regions dominate after thermal cleaning of shallower levels. These quasi-stable E intervals indicate the presence of thermally distinct trapping regions rather than a

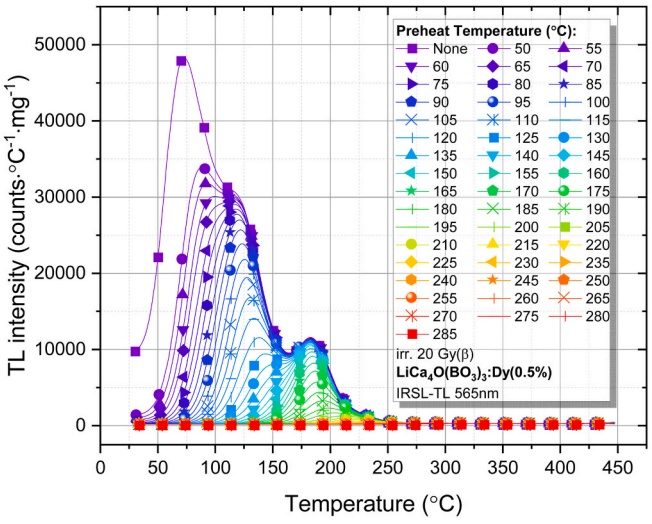

(a)

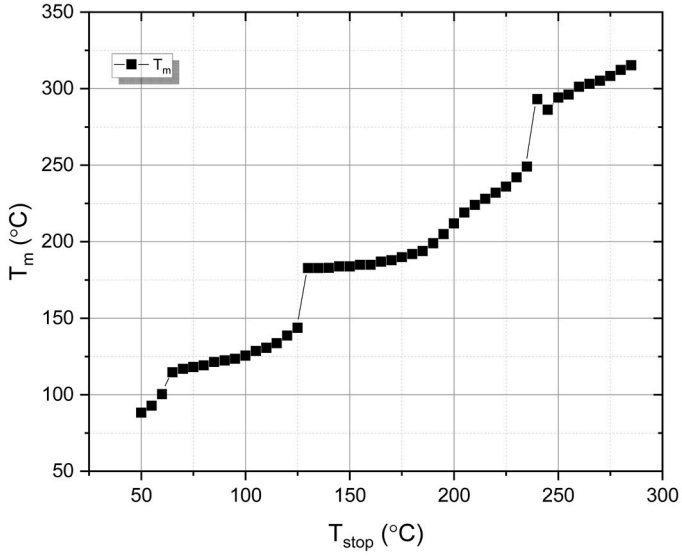

(b)

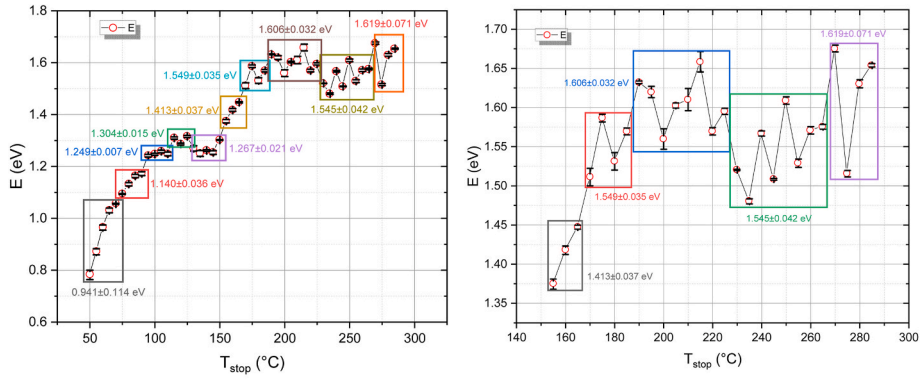

(c) (d)

Fig. 7. (a) TL glow curves of $LiCa_4O(BO_3)_3:Dy^{3+}$ (0.5 wt%) after successive preheating at different T_{stop} temperatures, showing progressive removal of low-temperature components. (b) Corresponding T_m–T_{stop} plot indicating multiple trapping levels and a mixed trap structure. **(c)** Activation energy (E) as a function of T_{stop} derived from successive preheating analysis, showing stepwise variations that reflect the presence of multiple thermally distinct trapping levels within the mixed trap hierarchy of $LiCa_4O(BO_3)_3:Dy^{3+}$ (0.5 wt%). (d) Refined E–T_{stop} behaviour at higher T_{stop} after progressive preheating, highlighting quasi-stable activation-energy intervals of deeper trap groups.

single uniform trap depth. Nevertheless, such stepwise behaviour should be regarded as indicative of trap grouping rather than definitive proof of fully isolated discrete levels, since similar E–T_{stop} trends may also arise from strongly overlapping peaks or quasi-continuous trap distributions.

Considering the pronounced overlap of the ~75, ~112 and ~182 °C components in the present glow curves, the overall T_m–T_{stop} and E–T_{stop} behaviour consistently supports a mixed trap hierarchy composed of shallow, intermediate and deeper trapping levels. Similar complex multi-component trap structures have been reported for lithium borate systems, including $Li_2B_4O_7$:Cu,Ag and Dy-doped lithium borates [11, 19], where TM–Tstop analysis was typically supported by CGCD to resolve overlapping contributions [42].

In order to further refine the trap-structure interpretation, the evolution of activation energy after systematic preheating is presented in Fig. 7d. Compared with the broader E–T_{stop} trend shown previously, the refined analysis highlights more clearly defined quasi-stable E intervals following the progressive removal of shallower components. These clustered E regions further substantiate the presence of multiple thermally distinguishable trapping domains.

Notably, the persistence of discrete E plateaus after successive thermal cleaning suggests that deeper trap groups become dominant once overlapping shallow contributions are suppressed. However, consistent with the limitations of T_m–T_{stop} methodology, these E clusters should be interpreted as indicative of thermally grouped trap regions rather than definitive evidence of isolated single trapping levels. Similar stepwise E evolution in lithium borates has been associated with mixed-trap hierarchies where overlapping discrete peaks and quasi-continuous distributions may coexist.

The refined E–T_{stop} behaviour therefore strengthens the interpretation of a multi-level trap hierarchy in $LiCa_4O(BO_3)_3$:Dy^{3+} and provides qualitative guidance for subsequent deconvolution analysis, without imposing rigid constraints on the exact number of trapping components, but instead defining physically meaningful energy intervals to be tested in subsequent CGCD analysis.

4.3. CGCD analysis

The TL glow curves of $LiCa_4O(BO_3)_3$:Dy^{3+} (0.5 wt%) exhibit pronounced asymmetry and significant peak overlap, indicating that the measured signal arises from multiple trapping levels rather than a single kinetic process. To separate these overlapping contributions and obtain individual trap parameters, CGCD was performed.

Deconvolution was applied to glow curves recorded both before and after preheating treatments in order to evaluate the roles of shallow and thermally stable traps. The analysis was carried out using the *tgcd* package implemented in the R environment [43].

Each component was fitted assuming general-order kinetics (GOK) [44]. The TL intensity for a single GOK peak is expressed as:

$$I(T) = I_m \exp\left(\frac{E}{kT_m^2}(T - T_m)\right)\left[\frac{1}{b} + \frac{b-1}{b}\exp\left(\frac{E}{kT_m^2}(T - T_m)\right)\right]^{-\frac{b}{b-1}} \quad (4)$$

where E is the activation energy, T_m is the peak maximum temperature, b is the kinetic order, k is the Boltzmann constant, and I_m is the maximum intensity.

The number of components was increased progressively and retained only when it produced a significant improvement in fit quality while maintaining physically reasonable parameter values consistent with the trap structure inferred from the T_m–T_{stop} and E–T_{stop} analyses.

The CGCD results obtained before and after preheating are presented in Fig. 8a and b, with the corresponding kinetic parameters summarized in Tables 2 and 3, respectively.

Prior to preheating (Fig. 8a), the TL glow curve exhibits pronounced asymmetry and a broad composite structure that is satisfactorily resolved into ten individual components (F.O.M. = 1.28%). The low-temperature region (≈66–110 °C) is described by four peaks with

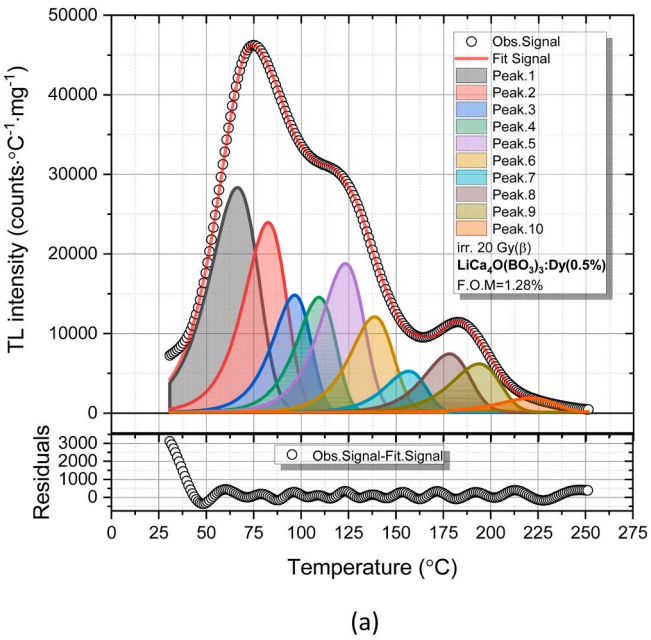

(a)

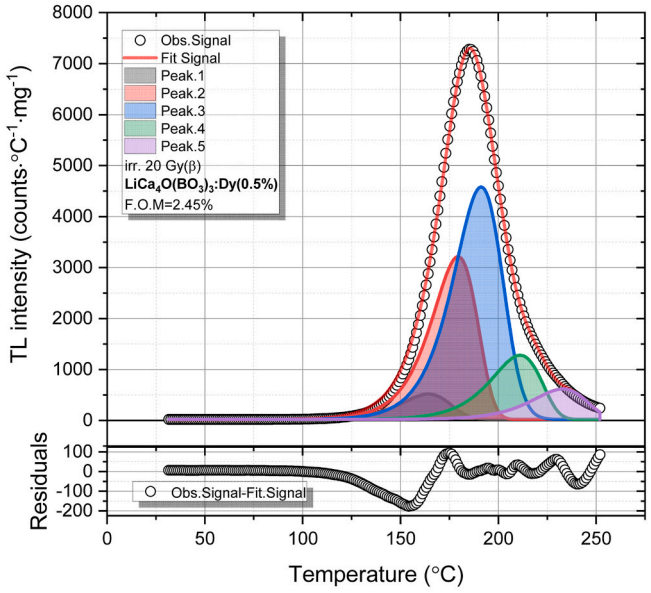

(b)

Fig. 8. (a) CGCD of the TL glow curve of $LiCa_4O(BO_3)_3$:Dy^{3+} (0.5 wt%) before preheating (b) after preheating.

activation energies ranging from 0.85 to 1.31 eV, corresponding to shallow and thermally less stable trapping levels. In the intermediate temperature range (≈123–157 °C), three additional components with activation energies between ~1.30 and 1.58 eV are identified, representing moderately stable traps. The high-temperature region (≈178–220 °C) is dominated by three deeper components with activation energies in the range of ~1.51–1.65 eV, associated with thermally more stable and dosimetrically relevant trapping levels. The kinetic order parameter b varies between 1.05 and 1.21, indicating slight deviation from ideal first-order kinetics and supporting a low-retrapping general-order behaviour. The frequency factors (10^{11}–10^{17} s^{-1}) fall within typical ranges reported for borate phosphors, supporting the physical plausibility of the extracted parameters.

After preheating (Fig. 8b), the glow curve becomes significantly simplified and can be adequately described using five components (F.O.

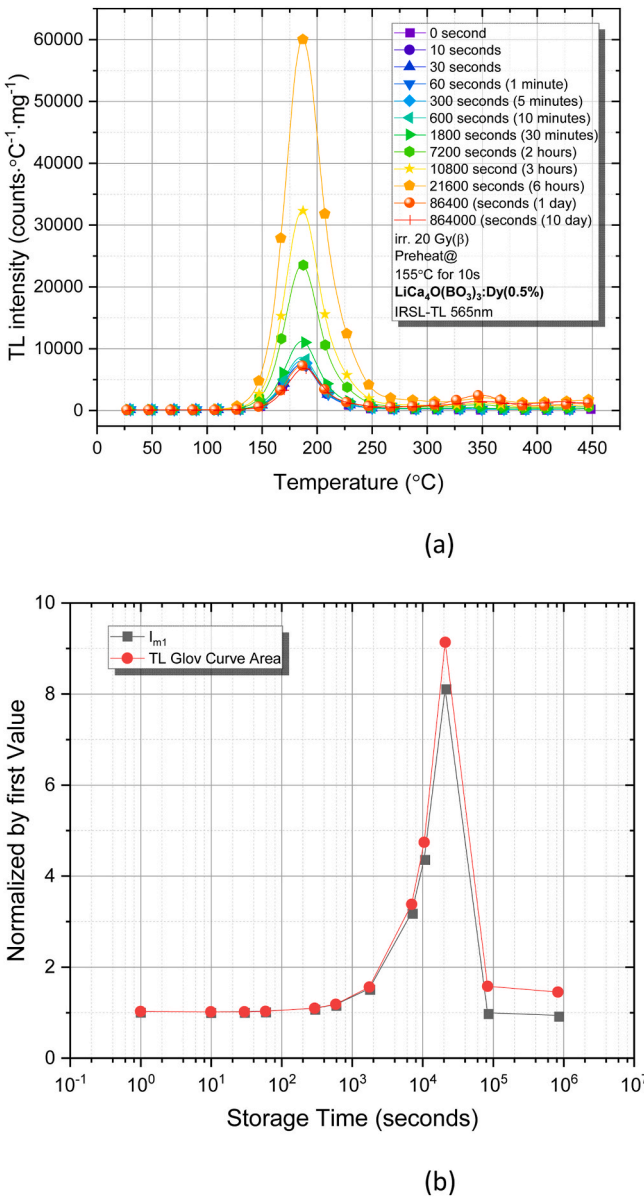

Fig. 9. (a) TL glow curves of $LiCa_4O(BO_3)_3:Dy^{3+}$ (0.5 wt%) recorded at different storage times (0 s to 10 days) after 20 Gy β-irradiation, showing non-monotonic fading behaviour of the main peak at ~185 °C. (b) Normalized main-peak temperature (T_m) and integrated TL glow-curve area as a function of storage time.

M. = 2.45%). The shallow low-temperature peaks observed before preheating are largely suppressed, consistent with the removal of thermally unstable traps as indicated by the T_m–T_{stop} analysis. The remaining peaks exhibit activation energies concentrated in the range of 1.44–1.67 eV, confirming that the post-preheating glow curve is dominated by deeper and more thermally stable trapping levels. The principal dosimetric peak around 180–233 °C remains clearly resolved, with kinetic order parameters close to unity ($b \approx 1.01$–1.19), again indicating general-order kinetics with limited retrapping.

It should be noted that the activation energies obtained from CGCD (1.44–1.67 eV) are slightly higher than those derived from the variable heating-rate analysis (≈1.2–1.26 eV). Such differences are frequently observed in complex and partially overlapping glow curves, where VHR yields an effective activation energy associated with the dominant trap group, whereas CGCD resolves thermally grouped components that may include deeper sub-levels within the same hierarchical structure. Considering experimental uncertainty, peak overlap effects and model dependence, the obtained values remain physically compatible and mutually supportive.

Importantly, the selection of ten components prior to preheating was not arbitrary but guided by both the pronounced asymmetry of the experimental glow curve and the independently inferred trap regions from the T_m–T_{stop} and E–T_{stop} analyses. The progressive inclusion of components was terminated once further additions did not yield a statistically meaningful improvement in the figure of merit (F.O.M.) or resulted in physically unrealistic parameter values. Moreover, the systematic reduction to five components after preheating provides internal validation of the deconvolution approach: shallow, thermally unstable peaks identified in the initial fit disappear consistently following thermal cleaning, while deeper components remain stable. This coherent evolution across independent analyses (T_m–T_{stop}, preheating behaviour, and CGCD) supports the interpretation of a multi-level trap hierarchy rather than mathematical overfitting. Nevertheless, glow-curve deconvolution in strongly overlapping borate systems remains inherently non-unique; therefore, the extracted components should be interpreted as physically consistent trap groups within a constrained kinetic framework, rather than uniquely resolved discrete trapping levels.

It should be noted that glow-curve deconvolution (CGCD) is inherently non-unique, and the number and parameters of the fitted components may depend on the selected fitting procedure and initial constraints. In this study, the deconvolution was guided and constrained by physically meaningful parameter ranges and by consistency with the expected TL kinetic behaviour, in order to obtain a realistic representation of the glow-curve structure rather than a purely mathematical fit. Similarly, the T_m–T_{stop} method does not always produce well-defined plateau regions, particularly in systems with closely spaced trap levels or significant peak overlap. In such cases, gradual variations in the T_m–T_{stop} curve may still reflect a distributed or mixed trap system rather than discrete, well-isolated traps. Therefore, the interpretation of the trap structure in the present work is based on the combined evaluation of CGCD, variable heating-rate measurements, and T_m–T_{stop} analyses, which together provide a consistent and physically meaningful description of the underlying trapping system, despite the known

Table 2
Kinetic parameters obtained from CGCD analysis of the TL glow curve of $LiCa_4O(BO_3)_3:Dy^{3+}$ (0.5 wt%) before preheating, including activation energy (E), kinetic order (b), peak temperatures (T_m, T_{m1}, T_{m2}), symmetry factor (μ), and frequency factor (s).

•	E_a (eV)	b	T_m (°C)	T_{m1} (°C)	T_{m2} (°C)	μ	s (s^{-1})
1st Peak	0.85	1.14	66.6706	49.0022	79.5302	0.41307	7.39×10^{11}
2nd Peak	1.09	1.15	82.85	67.653	93.9639	0.41975	5.34×10^{14}
3rd Peak	1.25	1.08	96.85	82.7734	106.777	0.41065	2.24×10^{16}
4th Peak	1.31	1.09	109.7312	95.3083	119.9549	0.40715	3.61×10^{16}
5th Peak	1.30	1.13	123.6583	107.902	135.0683	0.41037	6.17×10^{15}
6th Peak	1.44	1.17	139.0908	123.5931	150.5392	0.4312	7.84×10^{16}
7th Peak	1.58	1.07	157.0413	142.0243	167.5757	0.41703	6.39×10^{17}
8th Peak	1.65	1.21	178.6441	162.2506	190.9892	0.41996	4.73×10^{17}
9th Peak	1.61	1.12	194.2344	176.5106	206.999	0.42898	3.02×10^{16}
10th Peak	1.51	1.05	221.85	201.1504	236.2112	0.40761	3.37×10^{14}

Table 3
Kinetic parameters derived from CGCD analysis of the TL glow curve of $LiCa_4O(BO_3)_3:Dy^{3+}$ (0.5 wt%) after preheating, showing the remaining thermally stable components and their corresponding E, b, T_m, T_{m1}, T_{m2}, μ, and s values.

•	E_a (eV)	b	T_m (°C)	T_{m1} (°C)	T_{m2} (°C)	μ	s (s^{-1})
1st Peak	1.44	1.16	164.85	147.3972	177.6776	0.42792	6.40×10^{15}
2nd Peak	1.58	1.04	180.057	163.5085	191.4718	0.42026	6.62×10^{16}
3rd Peak	1.65	1.19	191.85	174.5669	204.7425	0.43156	1.34×10^{17}
4th Peak	1.61	1.01	211.85	193.3331	224.3324	0.40686	6.67×10^{15}
5th Peak	1.67	1.07	233.85	214.115	247.6915	0.41611	5.99×10^{15}

limitations of each individual method.

5. Post-irradiation temporal evolution and fading behaviour

$LiCa_4O(BO_3)_3:Dy^{3+}$ (0.5 wt%) exhibits a clear hierarchy of shallow, intermediate and deep trapping levels with strong peak overlap and mixed-trap interactions. Previous preheating and T_m–T_{stop} analyses demonstrated that progressive thermal cleaning removes shallow components while deeper structures persist, and that E–T_{stop} evolution proceeds in stepwise, quasi-stable intervals consistent with thermally grouped trap regions rather than a single uniform depth [16,45]. As shown in Fig. 9, the fading experiment reveals a two-stage temporal evolution of the main dosimetric peak (~185 °C): (i) a monotonic intensity increase during the first several hours of storage, followed by (ii) a subsequent long-term decrease. Importantly, the peak maximum temperature remains essentially constant during storage. The invariance of T_m indicates that the trap depth associated with the dosimetric peak does not change, and that the observed intensity variation is not related to structural modification or formation of new traps, but rather to redistribution of charge populations among pre-existing trapping states. The absence of any measurable shift in T_m during storage further supports that the dominant dosimetric trap depth remains unchanged, reinforcing the redistribution hypothesis rather than structural evolution.

Within a mixed-trap borate system, such early post-irradiation build-up can be physically interpreted as delayed charge migration from shallow or metastable traps toward deeper, thermally stable dosimetric traps [46,47]. Slow inter-trap transfer at room temperature, possibly mediated by defect clusters involving Dy^{3+} and charge-compensation centres, may progressively increase the occupancy of the ~185 °C trap. Notably, after the applied preheating protocol the glow curve is dominated by a single main peak (~185 °C), implying that the early-time intensity build-up primarily reflects redistribution processes within the trap–recombination network feeding this dosimetric peak rather than evolving contributions from separate low-temperature components. After this metastable equilibration stage, conventional thermal detrapping and recombination processes dominate, leading to long-term fading. It should be emphasized that post-irradiation intensity build-up is not widely reported as a generic feature of rare-earth-doped borates, where monotonic fading is more commonly described [18]. Therefore, the present behaviour is best regarded as system-specific and consistent with strong inter-trap coupling in a hierarchical trapping network, rather than as a universal property of Dy-borate phosphors.

While the proposed interpretation is physically plausible and internally consistent with T_m–T_{stop}, E–T_{stop} and CGCD results, alternative mechanisms such as slow room-temperature detrapping combined with competitive recombination or defect reconfiguration cannot be entirely excluded without dedicated time-resolved or isothermal TL investigations [48,49].

The two-stage temporal behaviour could, in principle, be described by a coupled rate-equation model involving shallow-to-deep trap transfer followed by conventional thermal detrapping. Although such modelling is beyond the scope of the present study, the observed time scale of intensity build-up is compatible with thermally assisted redistribution among traps with activation energies in the 1.0–1.3 eV range.

The observed two-stage storage behaviour is consistent with the trap hierarchy revealed by the CGCD analysis. Prior to preheating, the presence of multiple shallow and intermediate components suggests that a fraction of the charge is initially stored in metastable traps, which may progressively transfer to deeper dosimetric traps during early storage. The subsequent dominance of deeper components after preheating further supports the interpretation that the delayed intensity build-up of the ~185 °C peak arises from inter-trap redistribution within a mixed-trap framework rather than from the formation of new trapping centres.

From a dosimetric perspective, the absence of any observable shift in the peak maximum temperature (T_m) during storage, together with the dominance of the high-temperature TL peak after preheating, indicates that the main trapping level remains thermally stable and suitable for reliable dose evaluation over the investigated storage period.

6. Conclusions

$LiCa_4O(BO_3)_3:Dy^{3+}$ (0.5 wt%) exhibits a well-defined main dosimetric TL peak at ~185 °C with dose-independent peak temperature and an extended quasi-linear dose response ($b \approx 1.07$–1.16) over 1.4–150.1 Gy, indicating a thermally robust trapping level suitable for medium-dose applications. Heating-rate analyses using the Hoogenstraaten and Booth–Bohun–Parfianovitch approaches yield consistent activation energies of $E \approx 0.86$–1.26 eV and frequency factors on the order of 10^{13} s^{-1}, values physically reasonable for a relatively deep dosimetric trap and compatible with good room-temperature stability under the applied preheat–readout protocol. T_m–T_{stop} and E–T_{stop} analyses reveal stepwise, quasi-stable energy intervals, supporting a mixed trap hierarchy comprising shallow, intermediate and deep trapping regions rather than a single uniform depth distribution. Within this framework, CGCD solutions resolving ten components before preheating and five deeper components after preheating provide a physically consistent though inherently non-unique representation of thermally grouped trap families, confirming that post-preheat glow curves are dominated by deeper, more stable trapping levels. The observed two-stage post-irradiation evolution of the ~185 °C peak early intensity build-up followed by long-term fading at essentially constant T_m is consistent with mixed-trap kinetics involving delayed inter-trap charge redistribution and subsequent conventional thermal detrapping. Nevertheless, alternative mechanisms such as slow room-temperature detrapping or defect reconfiguration cannot be excluded without dedicated time-resolved or isothermal TL investigations. Overall, the combined kinetic and dosimetric characteristics indicate that $LiCa_4O(BO_3)_3:Dy^{3+}$ is a promising borate-based TL phosphor with favorable properties for practical dose recording applications.

CRediT authorship contribution statement

K. Bulcar: Methodology, Investigation, Formal analysis. **E.A. Cin:** Methodology, Investigation, Formal analysis. **Jabir Hakami:** Methodology, Investigation, Conceptualization. **Abeer S. Altowyan:** Writing – original draft, Methodology, Investigation, Funding acquisition, Formal analysis. **M.B. Coban:** Methodology, Investigation, Formal analysis. **U. H. Kaynar:** Methodology, Investigation, Data curation. **M. Topaksu:** Methodology, Conceptualization. **N. Can:** Writing – review & editing,

Writing – original draft, Supervision.

Declaration of competing interest

The authors declare that they have no known competing financial interests or personal relationships that could have appeared to influence the work reported in this paper.

Acknowledgements

The authors acknowledge the Princess Nourah bint Abdulrahman University Researchers Supporting Project (Project No. PNURSP2026R16), Princess Nourah bint Abdulrahman University, Riyadh, Saudi Arabia.

Data availability

Data will be made available on request.

References

[1] B.A. Kumar, P.H. Bindu, Advances in borate- and phosphate-based TL materials for in vivo dosimetry, J. Korean Ceram. Soc. 59 (2022) 537–550, https://doi.org/10.1007/s43207-022-00240-x.

[2] P.D. Sahare, M. Singh, P. Kumar, Synthesis and TL characteristics of MgB_4O_7:Mn, Tb phosphor, J. Lumin. 160 (2015) 158–164, https://doi.org/10.1016/j.jlumin.2014.11.042.

[3] Y. Kitagawa, E.G. Yukihara, S. Tanabe, Development of Ce^{3+} and Li^{+} co-doped magnesium borate glass ceramics for optically stimulated luminescence dosimetry, J. Lumin. 232 (2021) 117847, https://doi.org/10.1016/j.jlumin.2020.117847.

[4] Z.G. Portakal Uçar, Thermoluminescence characteristics and kinetic analysis of beta irradiated $Ca_4LaO(BO_3)_3$ phosphor, Cumhur. Sci. J. 42 (2021) 702–714, https://doi.org/10.17776/csj.929279.

[5] L.H. Jiang, Y.L. Zhang, C.Y. Li, R. Pang, J.Q. Hao, Q. Su, Thermoluminescence characteristics of rare-earth-doped $LiCaBO_3$ phosphor, J. Lumin. 128 (2008) 1904–1908, https://doi.org/10.1016/j.jlumin.2008.05.017.

[6] A.S. Altowyan, M. Sonsuz, U.H. Kaynar, J. Hakami, Z.G. Portakal-Uçar, M. Ayvacikli, M. Topaksu, N. Can, Synthesis and thermoluminescence behavior of novel Sm^{3+} doped $YCa_4O(BO_3)_3$ under beta irradiation, Ceram. Int. 50 (2024) 19681–19691, https://doi.org/10.1016/j.ceramint.2024.03.089.

[7] M. Oglakci, S. Akça-Özalp, Z.G. Portakal-Uçar, V. Correcher, J.F. Benavente, M. Sonsuz, N. Can, Y.Z. Halefoglu, M. Topaksu, Thermoluminescence study of Nd^{3+} doped lanthanum tri-borate phosphor, J. Alloys Compd. 1013 (2025) 178570, https://doi.org/10.1016/j.jallcom.2025.178570.

[8] M. Jena, D. Sen, M. Zulfequar, K. Asokan, A. Pandey, Study of the thermoluminescence properties of γ and UV-C irradiated Li_3PO_4: dy synthesized by solid state diffusion method, J. Alloys Compd. 955 (2023) 170077, https://doi.org/10.1016/j.jallcom.2023.170077.

[9] J. Sharma Neharika, V. Sharma, A.K. Bedyal, H.C. Swart, V. Kumar, Synthesis and thermoluminescence studies of UV-C exposed $Li_4Ca(BO_3)_2$: Dy^{3+} phosphors, Vacuum 156 (2018) 370–374, https://doi.org/10.1016/j.vacuum.2018.08.003.

[10] V.S. A, T. Chennappa, K. Naregundi, A. Princy, S.M.M. Kennedy, A.S. Altowyan, M. I. Sayyed, S.D. Kamath, Unveiling highly sensitive Dy^{3+} doped $BaMgAl_{10}O_{17}$ phosphor's thermoluminescence trap features and temperature dependent luminescence for solid state lighting applications, Phys. Scripta 99 (2024) 085909, https://doi.org/10.1088/1402-4896/ad5876.

[11] T. Ngoc, N.X. Ca, N.V. Ha, T.T.C. Thuy, N.T. Huong, L.D. Thanh, N. Van Nghia, P. Van Do, Thermoluminescence properties of the $Li_2B_4O_7$:Dy^{3+},Ce^{3+} glasses and their application potential in the dosimetry field, Opt. Mater. (Amst). 158 (2025) 116443, https://doi.org/10.1016/j.optmat.2024.116443.

[12] Y. Alajlani, M. Oglakci, K. Bulcar, Ü.H. Kaynar, Z.G. Portakal-Uçar, H.J. Alathlawi, M. Ayvacikli, M. Topaksu, N. Can, Anomalous heating rate effect in $GdAl_3(BO_3)_4$: Dy^{3+} under beta radiation stimulation: analysis of dose response and kinetic parameters, Ceram. Int. 49 (2023) 39967–39978, https://doi.org/10.1016/j.ceramint.2023.09.313.

[13] K. Bulcar, M. Oglakci, U.H. Kaynar, M. Ayvacikli, G. Souadi, M. Topaksu, N. Can, Thermoluminescence glow curve analysis and evaluation of trapping parameters of dysprosium doped lanthanum calcium borate $La_2CaB_{10}O_{19}$, Nucl. Instrum. Methods Phys. Res. Sect. B Beam Interact. Mater. Atoms 489 (2021) 58–68, https://doi.org/10.1016/j.nimb.2020.12.023.

[14] A.R. Beck, S. Das, J. Manam, Temperature dependent photoluminescence of Dy^{3+} doped $LiCaBO_3$ phosphor, J. Mater. Sci. Mater. Electron. 28 (2017) 17168–17176, https://doi.org/10.1007/s10854-017-7645-4.

[15] A.S. Altowyan, Ü.H. Kaynar, K. Bulcar, M. Oglakci, Z.G. Portakal-Uçar, J. Hakami, M. Topaksu, N. Can, Unusual heating rates, dose responses and kinetic parameters detected on thermoluminescence from $YAl_3(BO_3)_4$:Sm^{3+} phosphors, Ceram. Int. 49 (2023) 33291–33304, https://doi.org/10.1016/j.ceramint.2023.08.038.

[16] O. Madkhali, K. Bulcar, A. Barad, T. Zelai, G. Souadi, H.J. Alathlawi, U.H. Kaynar, M. Topaksu, N. Can, Thermoluminescence behaviour and kinetic analysis of a novel Tb^{3+}-Doped $LaCa_4O(BO_3)_3$ phosphor: impacts of heating rates and dose, Mater. Sci. Semicond. Process. 187 (2025) 109132, https://doi.org/10.1016/j.mssp.2024.109132.

[17] B. Zhai, M.M. Chen, Y.M. Huang, Photoluminescence and afterglow of Dy^{3+} doped $CaAl_2O_4$ derived via sol–gel combustion, RSC Adv. 12 (2022) 31757–31768, https://doi.org/10.1039/D2RA05008K.

[18] M. Oglakci, Z.G. Portakal-Uçar, S. Akça-Özalp, V. Correcher, J.F. Benavente, M. Sonsuz, N. Can, Y.Z. Halefoglu, M. Topaksu, Thermoluminescence behavior of Ce^{3+} doped lanthanum tri-borate phosphor for dosimetry applications, Ceram. Int. 49 (2023) 36092–36102, https://doi.org/10.1016/j.ceramint.2023.08.288.

[19] N. El-Faramawy, A. El-Naggar, C. Woda, M. El-Kinawy, Investigation of TL dosimetric parameters of lithium borate glass doped with dysprosium, Opt. Mater. 113 (2021) 110672, https://doi.org/10.1016/j.optmat.2020.110672.

[20] A. Oza, V. Ojha, S. Dhale, S. Dhoble, Photoluminescence and thermoluminescence in Dy^{3+}-, Ce^{3+}-, and Tb^{3+}-activated MgB_4O_7 phosphor for dosimetry application, Luminescence 37 (2022) 1563–1574, https://doi.org/10.1002/bio.4332.

[21] G.I. Efenji, I.S. Bin Mustapha, N.N. Yusof, R.J. Anthony, F.A. Kamgba, U.P. O, T. Hussein Khazaalah, M. Jamil, M.F. Izwan, U.S. Aliyu, N.S. Ezra, A.O. Oke, H. Salah Naeem, A. Muhammad, A.S.A. Idriss, Characteristics and dosimetric properties of tissue-equivalent thermoluminescent glass detector based on Al-Li-Zn, borate oxide dope Dy^{3+}, Sci. Technol. Indones 9 (2024) 965–980, https://doi.org/10.26554/sti.2024.9.4.965-980.

[22] M. Sen, R. Shukla, V. Sathian, M.S. Kulkarni, A.K. Tyagi, Thermoluminescence based personnel neutron dosimetry study of LiMgBO3:Dy3+, Ceram. Int. 46 (2020) 20236–20242, https://doi.org/10.1016/j.ceramint.2020.05.105.

[23] M. Bakr, Z.G. Portakal-Uçar, M. Yüksel, Ü.H. Kaynar, M. Ayvacikli, S. Benourdja, A. Canimoglu, M. Topaksu, A. Hammoudeh, N. Can, Thermoluminescence properties of beta particle irradiated $Ca_3Al_2O_6$ phosphor relative to environmental dosimetry, J. Lumin. 227 (2020) 117565, https://doi.org/10.1016/j.jlumin.2020.117565.

[24] W. Li, S. Wu, J. Ren, P. Xiong, Defects in inorganic mechanoluminescent phosphors: insights and impacts, Adv. Funct. Mater. 35 (2025), https://doi.org/10.1002/adfm.202506198.

[25] V. Vitola, D. Millers, I. Bite, K. Smits, A. Spustaka, Recent progress in understanding the persistent luminescence in $SrAl_2O_4$:Eu,Dy, Mater. Sci. Technol. 35 (2019) 1661–1677, https://doi.org/10.1080/02670836.2019.1649802.

[26] P. Dewangan, D.P. Bisen, N. Brahme, S. Sharma, Structural characterization and luminescence properties of Dy^{3+} doped $Ca_3MgSi_2O_8$ phosphors, J. Alloys Compd. 777 (2019) 423–433, https://doi.org/10.1016/j.jallcom.2018.10.390.

[27] D. Gao, Y. Li, L. Cheng, S. Liu, S. Xu, X. Li, J. Zhang, X. Zhang, Y. Cao, Y. Wang, X. Wang, Y. Zhang, X. Sha, L. Wang, B. Chen, Concentration effects of fluorescence quenching and optical transition properties of Dy^{3+} doped $NaYF_4$ phosphor, J. Alloys Compd. 895 (2022) 162616, https://doi.org/10.1016/j.jallcom.2021.162616.

[28] W. Tang, Q. Guo, K. Su, H. Liu, Y. Zhang, L. Mei, L. Liao, Structure and photoluminescence properties of Dy^{3+} doped phosphor with whitlockite structure, Materials 15 (2022) 2177, https://doi.org/10.3390/ma15062177.

[29] S. Yan, S. Liu, Y. Sun, S. Zhang, G. Chen, Z. Zheng, Multi behaviors of Dy^{3+} for improving the luminescence properties of Pr^{3+}-activated $Sr_3Al_2O_6$ orange-reddish phosphors, Chem. Phys. Lett. 807 (2022) 140071, https://doi.org/10.1016/j.cplett.2022.140071.

[30] J.A. Jiménez, V. Hedge, C.S.D. Viswanath, R. Amesimenu, Insights into the structural, Thermal/Dilatometric, and optical properties of Dy^{3+} -Doped phosphate glasses for lighting applications, ACS Phys. Chem. Au 4 (2024) 720–735, https://doi.org/10.1021/acsphyschemau.4c00066.

[31] H. Zhang, B. Cao, Z. Liao, Y. Yang, J. Zhang, L. Li, Y. Cong, Y. He, Z. Zhang, Z. Feng, B. Dong, Energy transfer mechanism and new ratiometric thermometry strategy by the blue and yellow emissions of Dy, Ceram. Int. 48 (2022) 29838–29846, https://doi.org/10.1016/j.ceramint.2022.06.248.

[32] P.D. Townsend, Y. Wang, S.W.S. McKeever, Spectral evidence for defect clustering: relevance to radiation dosimetry materials, Radiat. Meas. 147 (2021) 106634, https://doi.org/10.1016/j.radmeas.2021.106634.

[33] J.M. Kalita, M.L. Chithambo, Thermoluminescence of α-Al_2O_3:C,Mg: kinetic analysis of the main glow peak, J. Lumin. 182 (2017) 177–182, https://doi.org/10.1016/j.jlumin.2016.10.031.

[34] R. Chen, J.L. Lawless, V. Pagonis, On the various-heating-rates method for evaluating the activation energies of thermoluminescence peaks, Radiat. Meas. 150 (2022) 106692, https://doi.org/10.1016/j.radmeas.2021.106692.

[35] R. Chen, S.W.S. McKeever, Theory of Thermoluminescence and Related Phenomena, World Scientific, 1997, https://doi.org/10.1142/2781.

[36] S.W.S. McKeever, Thermoluminescence of Solids, Cambridge University Press, 1985, https://doi.org/10.1017/CBO9780511564994.

[37] G. Kitis, J.W.N. Tuyn, A simple method to correct for the temperature lag in TL glow-curve measurements, J. Phys. D Appl. Phys. 31 (1998) 2065–2073, https://doi.org/10.1088/0022-3727/31/16/017.

[38] C. Furetta, Handbook of Thermoluminescence, World Scientific, 2003, https://doi.org/10.1142/5167.

[39] J.F. Benavente, J.M. Gómez-Ros, V. Correcher, Characterization of the thermoluminescence glow curve of $Li_2B_4O_7$:Cu,Ag, Radiat. Meas. 137 (2020) 106427, https://doi.org/10.1016/j.radmeas.2020.106427.

[40] J.F. Benavente, J.M. Gómez-Ros, A.M. Romero, Thermoluminescence glow curve deconvolution for discrete and continuous trap distributions, Appl. Radiat. Isot. 153 (2019) 108843, https://doi.org/10.1016/j.apradiso.2019.108843.

[41] A. Barad, M. Topaksu, J. Hakami, N. Can, Thermoluminescence kinetics in beta-irradiated novel $ZnGa_2O_4$:Eu^{3+} phosphor produced via gel combustion synthesis, Ceram. Int. 50 (2024) 11458–11468, https://doi.org/10.1016/j.ceramint.2024.01.046.

[42] S. Sarıkcı, M. Topaksu, M. Bakr, N. Can, Structural and analyses of thermoluminescence glow curves in Sm doped $SrGd_2O_4$ phosphor, J. Alloys Compd. 911 (2022) 165008, https://doi.org/10.1016/j.jallcom.2022.165008.

[43] J. Peng, Z. Dong, F. Han, Tgcd: an R package for analyzing thermoluminescence glow curves, SoftwareX 5 (2016) 112–120, https://doi.org/10.1016/j.softx.2016.06.001.

[44] J.M. Gomez Ros, G. Kitis, Computerised glow curve deconvolution using general and mixed order kinetics, Radiat. Protect. Dosim. 101 (2002) 47–52, https://doi.org/10.1093/oxfordjournals.rpd.a006029.

[45] S. Balci-Yegen, M. Yüksel, N. Kucuk, Y. Karabulut, M. Ayvacikli, N. Can, M. Topaksu, Thermoluminescence dose and heating rate dependence and kinetic analysis of ZnB_2O_4:0.05Dy^{3+} phosphor, Nucl. Instrum. Methods Phys. Res. Sect. B Beam Interact. Mater. Atoms 416 (2018) 50–54, https://doi.org/10.1016/j.nimb.2017.12.004.

[46] M.L. Chithambo, D.E. Folley, Dosimetric features, kinetics and mechanisms of thermoluminescence of tanzanite, Phys. B Condens. Matter 598 (2020) 412435, https://doi.org/10.1016/j.physb.2020.412435.

[47] J. Bierwagen, T. Delgado, G. Jiranek, S. Yoon, N. Gartmann, B. Walfort, M. Pollnau, H. Hagemann, Probing traps in the persistent phosphor $SrAl_2O_4$:Eu^{2+},Dy^{3+},B^{3+} - a wavelength, temperature and sample dependent thermoluminescence investigation, J. Lumin. 222 (2020) 117113, https://doi.org/10.1016/j.jlumin.2020.117113.

[48] K. Ozerskyi, Determination of correction factors and correction coefficients for calculations of the absorbed dose, Ukr. Metrol. J. (2024) 51–57, https://doi.org/10.24027/2306-7039.2.2024.307280.

[49] Y. Akter, A.M. Rahman, M.H. Sahadath, S. Yeasmin, N. Hassan, S. Banik, Z. Hossain, Thermoluminescence responses of TLD–100 subject to low dose irradiation, Dhaka Univ. J. Appl. Sci. Eng. 6 (2022) 59–63, https://doi.org/10.3329/dujase.v6i2.59219.